Journal of İstanbul Kültür University
2006/2 pp. 41-51

SPATIO-TEMPORAL PATTERNS IN A SEMICONDUCTOR-GAS-DISCHARGE SYSTEM: NUMERICAL SOLUTIONS AND STABILITY ANALYSIS IN 3D GEOMETRY

Ismail RAFATOV[1]

Abstract

We investigated the spatio-temporal patterns formation in the semiconductor-gas-discharge sys-tem consisting of a short gas-discharge layer sandwiched with a semiconductor layer between planar electrodes to which a dc voltage is applied, in three spatial dimensions. We define the model, identify its independent dimensionless parameters, and then present the results of the full time-dependent numerical solutions of the model as well as of a linear stability analysis of the stationary state. Numerical solutions and the results of the stability analysis agree well. Numerical results show that at parameter regime we investigated either purely Hopf bifurcation or Turing-Hopf bifurcation takes place.

***Key words**: Pattern formation, stability analysis, barrier discharge, modeling, numerical solution*

1. Introduction

Pattern forming system are well known in different branches of science, among them biology, chemistry, and physics [1]. The present work deals with the investigation of spatio-temporal patterns in semiconductor-gas- discharge systems. We focus on experiments performed in [2], where experimental system consisted of two parallel planar layers: a planar glow discharge layer with short length in the forward direction and wide lateral dimensions, which is coupled to a semiconductor layer with low conductivity. The whole

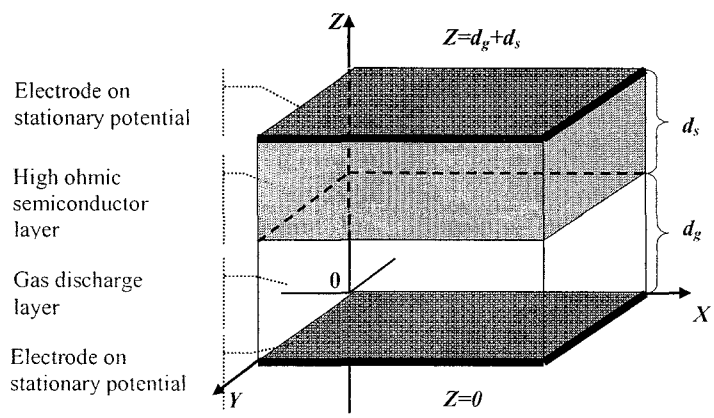

FIG. 1: The system of gas discharge and semiconductor.

[1]Physics Department, Middle East Technical University, 06531 Ankara

structure is sandwiched between two coplanar electrodes to which a DC voltage is applied.

Experiments showed that this system can exhibit a rich variety of structures: homogenous stationary and oscillating modes, patterns with spatial and spatio-temporal structure (stripes, spots, spirals in the plane orthogonal to the layers) [3]. In previous work [4, 5], authors concentrated on the purely temporal oscillations that occur in a spatially homogeneous mode, where the analysis was restricted to the direction normal to the layers, assuming homogeneity in the transversal direction. Results [4] showed that a simple two-component reaction-diffusion approximation for current and voltage in the gas discharge layer can not be sufficient to describe the oscillations, though such a model is suggested through similarities with patterns formed in a number of physical, chemical or biological systems like Belousov-Zhabotinski reaction, Rayleigh-Benard convection, patterns in bacterial colonies etc.

In [5] and [6], on the basis of the minimal model, results of one- and two-dimensional full time-dependent numerical solutions as well as a linear stability analysis of the stationary state were presented, which were found to be in very good agreement. Besides, qualitative and quantitative analysis of the solutions showed that this simplest model can reproduce the essential features of the experiments [2, 7].

The present work is the next extension of work [4, 5, 6]. Here, we continue the analysis of the gas discharge model, coupled to a high-Ohmic layer and driven by a stationary voltage, but now in three spatial dimensions: second transversal spatial dimension is added next to the previously investigated in [6] two-dimensional system

The paper is organized as follows. In Sec. 2 we introduce the model, perform dimensionless analysis, reduce the model by adiabatic elimination of electrons and formulate the problem in final form as an initial boundary value problem. In Sec. 3 we discuss dispersion relations obtained from the linear perturbation analysis about the stationary homogeneous solution. Numerical details for full pde system and numerical examples are described in Sec. 4. Finally, Sec. 5 contains the concluding remarks.

2. Model

In this section, we introduce the three-dimensional model for the glow discharge - semiconductor system. This model was previously investigated in planar quasi-one-dimensional geometry in [5], and in two-dimensional geometry in [6], as discussed in the Introduction.

2.1 Gas-Discharge and Semiconductor Layers

We derive the model as previously in [5] and [6]. The gas discharge part of the model consists of continuity equations for two charged species, namely, electrons and positive ions with particle densities n_e and n_i,

$$\partial_t n_e + \nabla \cdot \mathbf{\Gamma}_e = source\,,\ \partial_t n_i + \nabla \cdot \mathbf{\Gamma}_i = source\,, \qquad (1)$$

which are coupled to Poisson's equation for the electric field in electrostatic approximation,

$$\nabla \cdot \mathbf{E} = \frac{e}{\varepsilon_0}(n_i - n_e)\,,\ \mathbf{E} = -\nabla\Phi\,. \qquad (2)$$

Here, Φ is the electric potential, $\mathbf{E}$ is the electric field, e is the electron unite charge,

ε_0 is the dielectric constant, $\mathbf{\Gamma}_e$ and $\mathbf{\Gamma}_i$ are the particle current densities, which in the simplest approximation are described by drift only, where drift velocities are assumed to be linearly dependent on the local electric field with motilities $\mu_e >> \mu_i$:

$$\nabla \cdot \mathbf{\Gamma}_e = n_e \mu_e \mathbf{E}, \ \nabla \cdot \mathbf{\Gamma}_i = n_i \mu_i \mathbf{E}. \tag{3}$$

Two types of ionization processes are taken into account: the α process of electron impact ionization in the bulk of the gas, and the γ process of electron emission by ion impact onto the cathode. In a local field approximation, the α process determines the source terms in the continuity
equations (1):

$$source = |\mathbf{\Gamma}_e| \alpha(|\mathbf{E}|), \ \alpha(|\mathbf{E}|) = \alpha_0 \alpha(|\mathbf{E}|/E_0), \tag{4}$$

which, due to charge conservation, is identical for both equations. We use the classical Townsend approximation [8] for function

$$\alpha(|\mathbf{E}|/E_0) = \exp(-E_0/|\mathbf{E}|). \tag{5}$$

The semiconductor layer of thickness d_s is assumed to have a homogeneous and field-independent conductivity $\overline{\sigma}_s$ and dielectricity constant ε_s:

$$\mathbf{\Gamma}_s = \overline{\sigma}_s \mathbf{E}_s, \ q = \varepsilon_s \varepsilon_0 \nabla \mathbf{E}. \tag{6}$$

2.2 Boundary Conditions

The boundary conditions at the anode, $Z = 0$, describes the absence of ion emission. When diffusion is neglected, then the ion density vanishes,

$$\mathbf{\Gamma}_i(X,Y,0,t) = 0 \ \Rightarrow \ n_i(X,Y,0,t) = 0. \tag{7}$$

The boundary condition at the cathode, $Z = d_g$, describes the γ-process:

$$\mathbf{\Gamma}_e(X,Y,d_g,t) = \gamma |\mathbf{\Gamma}_i(X,Y,d_g,t)| \ \Rightarrow \ \mu_e n_e(X,Y,d_g,t) = \lambda \mu_i n_i(X,Y,d_g,t). \tag{8}$$

Across the boundary between gas layer and semiconductor layer, the electric potential is continuous while the jump of normal components of the electric field is determined by the surface charge:

$$q_b = (\varepsilon_s \varepsilon_0 \mathbf{E}_s - \varepsilon_0 \mathbf{E}_g) \cdot \hat{\mathbf{n}}, \tag{9}$$

where $\hat{\mathbf{n}}$ is a unit normal to the boundary surface and is directed from the gas to the semiconductor. Subscripts s and g refer to semiconductor and gas respectively. Applying charge conservation law at the boundary interface, we come to the jump condition in the following form:

$$q_b = q_b|_{t=0} + \int_0^t [(1+\gamma) e n_i \mu_i E_g - \overline{\sigma}_s E_g] \cdot \hat{\mathbf{n}} dt \tag{10}$$

Denoting applied DC voltage as U_t, due to gauge freedom, we have

$$\Phi(X,Y,0,t)=0,\ \Phi(X,Y,d_g+d_s,t)=-U_t. \qquad (11)$$

2.3 Dimensional Analysis

The dimensional analysis is performed as previously in [5]. We introduce the following dimensionless time, coordinates and fields

$r=\mathbf{R}/r_0$, $\tau=t/t_0$, $\sigma(\mathbf{r},t)=en_e(\mathbf{R},t)/q_0$, $\rho(\mathbf{r},t)=en_i(\mathbf{R},t)/q_0$,

$\mathcal{E}(\mathbf{r},t)=E(\mathbf{R},t)/E_0$,

measuring quantities in terms of the intrinsic parameters of the system

$$r_0=\frac{1}{\alpha_0},\ t_0=\frac{1}{\alpha_0\mu_e E_0},\ q_0=\varepsilon_0\alpha_0 E_0.$$

Here, $\mathbf{R}=X\hat{\mathbf{i}}+Y\hat{\mathbf{j}}+Z\hat{\mathbf{k}}$, $\mathbf{r}=x\hat{\mathbf{i}}+y\hat{\mathbf{j}}+z\hat{\mathbf{k}}$, where $\hat{\mathbf{i}}$, $\hat{\mathbf{j}}$, and $\hat{\mathbf{k}}$ are unit vectors.

The intrinsic dimensionless parameters of the gas discharge are the mobility ratio μ of the electrons and ions, $\mu=\mu_i/\mu_e$, and the length ratio L of the system size and inverse cross section of impact ionization, $L=d_g/r_0$. The dimensionless parameters of the semiconductor are conductivity $\sigma_s=\bar{\sigma}_s/\mu_e q_0$ and semiconductor layer $L_s=d_s/r_0$. Dimensionless capacitance and resistance can be written as $R_s=L_s/\sigma_s$ and $C_s=\varepsilon_s/L_s$. The total applied voltage can be rescaled as $\mathcal{U}_t=U_t/E_0 r_0$.

Our choice of parameters was guided by the experiments in [2] and taken as previously in [5] and [6]. We chose the secondary emission coefficient $\gamma=0.08$, the mobility ratio $\mu=0.0035$ for nitrogen, $\alpha_0=1/r_0=[27.78\ \mu\text{m}]^{-1}$, $E_0=10.26$ kV/cm, and the dimensionless system size $L=36$ which amounts to 1 mm at a pressure of 40 mbar. The value L_s for semiconductor layer thickness is 54. The dimensionless capacitance of the semiconductor is $C_s=0.243$. The value R_s for semiconductor resistance varies in the interval $[2\cdot10^5, 2\cdot10^6]$. A dimensionless total voltage $\mathcal{U}_t$ is in the range between 17.5 and 50. This corresponds to a GaAs layer with $\varepsilon_s=13.1$, conductivity $\bar{\sigma}_s=(2.6\times10^5\,\Omega\text{cm})^{-1}$ and thickness $d_s=1.5$ mm for the semiconductor layer, and a voltage range between 500 and 1425 V.

2.4 Reduction of the Model and Final Formulation of the Problem

Analogously to [5] and [6], we perform adiabatic elimination of the electrons. After substituting $s = \sigma/\mu$ and introducing a new time scale $\bar{\tau} = \mu\tau$, in the limit of $\mu \to 0$, the gas discharge part of the system have the form of

$$-\nabla(s\mathbf{E}) = s|\mathbf{E}|\alpha(|\mathbf{E}|),\ \partial_{\bar{\tau}}(\rho) + \nabla(\rho\mathbf{E}) = s|\mathbf{E}|\alpha(|\mathbf{E}|), \tag{12}$$

$$\nabla\mathbf{E} = \rho,\ \mathbf{E} = -\nabla\varphi. \tag{13}$$

For the semiconductor layer, the following equations are applied:

$$\nabla\mathbf{E} = 0,\ \mathbf{E} = -\nabla\varphi,\ j_s = \sigma_s\mathbf{E}. \tag{14}$$

The boundary conditions for the glow discharge are

$$\rho(x,y,0,\bar{\tau}) = 0,\ s(x,y,L,\bar{\tau}) = \gamma\rho(x,y,L,\bar{\tau}). \tag{15}$$

Condition for the charge on the semiconductor-gas boundary becomes

$$q_b(x,y,\bar{\tau}) = q_b(x,y,0) + \int_0^{\bar{\tau}} d\bar{\tau}\left[(1+\gamma)\left(\rho E_z\big|_{z=L^-} - \frac{\sigma_s}{\mu}E_z\big|_{z=L^+}\right)\right]. \tag{16}$$

At the anode and cathode, $z = 0$ and $z = L_z$, the electric potential is determined as $\varphi(x,y,0,t) = 0$ and $\varphi(x,y,L_z,t) = -\mathcal{U}_t$, respectively.

Finally, at the lateral boundaries, $x = 0$, $x = L_x$, and $y = 0$, $y = L_y$ we used periodical conditions for particle densities and electric potential,

$$\begin{aligned}
\rho(\mathbf{r},\bar{\tau})\big|_{x=0} &= \rho(\mathbf{r},\bar{\tau})\big|_{x=L_x},\\
s(\mathbf{r},\bar{\tau})\big|_{x=0} &= s(\mathbf{r},\bar{\tau})\big|_{x=L_x},\\
\varphi(\mathbf{r},\bar{\tau})\big|_{x=0} &= \varphi(\mathbf{r},\bar{\tau})\big|_{x=L_x}, \qquad (17)\\
\rho(\mathbf{r},\bar{\tau})\big|_{y=0} &= \rho(\mathbf{r},\bar{\tau})\big|_{y=L_y},\\
s(\mathbf{r},\bar{\tau})\big|_{y=0} &= s(\mathbf{r},\bar{\tau})\big|_{y=L_y},\\
\varphi(\mathbf{r},\bar{\tau})\big|_{y=0} &= \varphi(\mathbf{r},\bar{\tau})\big|_{y=L_y}. \qquad (18)
\end{aligned}$$

Here, $L_z = L + L_s$ and L_x denote the size of the system in z and x directions, respectively.

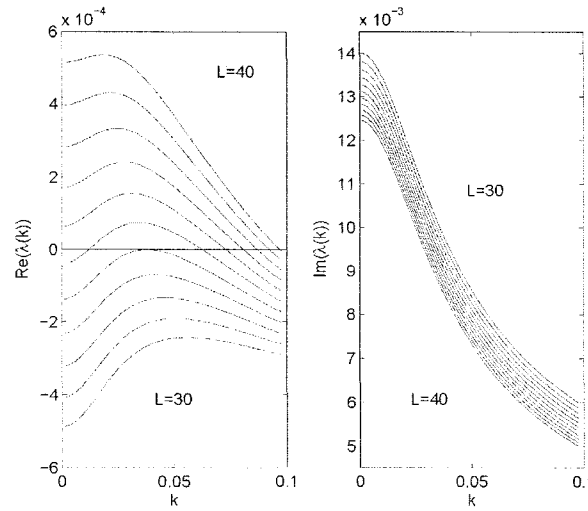

FIG. 2: Real and imaginary parts of the dispersion relation as functions of width of the gas layer L, where L varies from 30 to 40. L_s=54, R_s=2·10^6 and U_t=40. [6]

3. Spatio-Temporal Patterns: Linear Stability Analysis

Results of linear perturbation analysis, performed for transversal Fourier modes in [6], are applicable for the present three-dimensional case for the ansatz of the form

$$s(x,y,z,\bar{\tau}) = s_0(z) + s_1(z)\mathrm{e}^{\mathrm{i}(k_x x + k_y y)}\mathrm{e}^{\lambda\bar{\tau}}, \tag{19}$$

$$\rho(x,y,z,\bar{\tau}) = \rho_0(z) + \rho_1(z)\mathrm{e}^{\mathrm{i}(k_x x + k_y y)}\mathrm{e}^{\lambda\bar{\tau}}, \tag{20}$$

$$\varphi(x,y,z,\bar{\tau}) = \varphi_0(z) + \varphi_1(z)\mathrm{e}^{\mathrm{i}(k_x x + k_y y)}\mathrm{e}^{\lambda\bar{\tau}}, \tag{21}$$

with the only difference that wave-number k from the two-dimensional calculations [6] becomes $k = \sqrt{k_x^2 + k_y^2}$. Stationary solutions, which are obtained from the one-dimensional calculations, are denoted with the index 0. The index 1 denotes a small perturbation about the stationary solution.

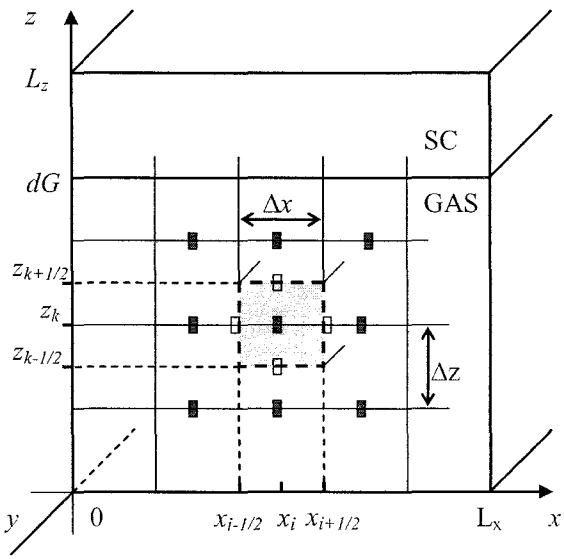

FIG. 3: Computational domain. Computational cell. Projection into XZ plane.

Dispersion curves, which derived from the eigenvalue problem, allow to determine whether a spatially homogeneous or spatially structured pattern can be expected to emerge from a perturbation of the homogeneous stationary state. In the last case, there will be a band of Fourier modes with positive growth rate $\mathrm{Re}(\lambda(k))$ with maximum for some non-vanishing k. Actually, for certain $k<<1$, a maximum of the real part of eigenvalue appears.

Fig. 2 shows the results of linear stability analysis for a particular set of parameters [6]. The maximal growth rate there is attained for a finite wavenumber. If the growth rate is positive, which is the case if the dimensionless width L of the gas discharge layer is larger than 34, then the stationary homogeneous system is unstable and the k with the maximal growth rate will dominate the behavior. Moreover, the frequency $\mathrm{Im}(\lambda(k))$ is finite. This means that the spatially modulated perturbation will not simply grow, but also oscillate in time.

The influence of conductivity and thickness of semiconductor layer etc. can be investigated in a similar manner.

4.1.1 Grid.

The computational domain is the rectangular region $[0,L_x]\times[0,L_y]\times[0,L_z]$ in the three dimensional Cartesian coordinate system (x,y,z), which consists on a planar layer of gas discharge, combined with a planar semiconductor layer (See figure 3).

We use a uniform vertex-centered grid in the 'longitudinal' z-direction with nodes

$$z_k = k\Delta z, \quad \Delta z = L_z/N, \quad k = 0,1,..,N,$$

and a uniform cell-centered grid with nodes

$x_i = (i-0.5)\Delta x$, $\Delta x = L_x/M_x$, $i = 1,2,..,M_x$ and $y_j = (j-0.5)\Delta y$, $\Delta y = L_y/M_y$, $j = 1,2,..,M_y$ in the 'transversal' x and y directions. The grid is spaced such that the internal border between semiconductor and gas region lies exactly on the grid plane.

Densities σ and ρ and electric potential φ are evaluated at the nodes of the grids, while the component $\mathcal{E}_x$, $\mathcal{E}_y$ and $\mathcal{E}_z$ of the electric field at the surfaces of the computational cell (figure 3).

4.1.2 Continuity Equation.

To obtain a finite-difference representation of equations (12), we first integrate them over the cell volume $x_{i-1/2} \le x \le x_{i+1/2}$, $y_{j-1/2} \le y \le y_{j+1/2}$, $z_{k-1/2} \le z \le z_{k+1/2}$. For the ion density equation we have

$$\frac{d\rho_{k,j,i}}{dt} = \frac{(\mathcal{E}_x\rho)_{k,j,i-1/2} - (\mathcal{E}_x\rho)_{k,j,i+1/2}}{\Delta x} + \frac{(\mathcal{E}_y\rho)_{k,j-1/2,i} - (\mathcal{E}_y\rho)_{k,j+1/2,i}}{\Delta y}$$

$$+ \frac{(\mathcal{E}_z\rho)_{k-1/2,j,i} - (\mathcal{E}_z\rho)_{k+1/2,j,i}}{\Delta z} + f_{k,j,i}. \qquad (22)$$

Note that the subscripts i and j refer to 'transversal', while k to 'longitudinal' direction, respectively, and f stands for the source term of equation (12).

The choice of $\rho_{k,j\pm1/2,i}$, $\rho_{k,j,i\pm1/2}$, and $\rho_{k\pm1/2,j,i}$ at the surfaces of the computational cell determines the discretization method for the convective terms in equation (22). We used the third-order upwind-biased scheme (See, e.g. [9], pp.83), which in the case of z-direction has a form of

$$(\mathcal{E}_z\rho)_{k+1/2,j,i} = \frac{1}{6}\Big[\mathcal{E}^+_{z\,k+1/2,j,i}\left(-\rho_{k-1,j,i} + 5\rho_{k,j,i} + 2\rho_{k+1,j,i}\right)$$

$$+ \mathcal{E}^-_{z\,k+1/2,j,i}\left(2\rho_{k,j,i} + 5\rho_{k+1,j,i} - \rho_{k+2,j,i}\right)\Big], \qquad (23)$$

where

$$\mathcal{E}^+_{z\,k+1/2,j,i} = \max(0,\mathcal{E}_{z\,k+1/2,j,i}), \quad \mathcal{E}^-_{z\,k+1/2,j,i} = \min(0,\mathcal{E}_{z\,k+1/2,j,i}),$$

with

$$\mathcal{E}_{z\,k+1/2,j,i} = \frac{\varphi_{k,j,i} - \varphi_{k+1,j,i}}{\Delta z}. \qquad (24)$$

In x-direction and y-direction the procedure is similar.

For the numerical time integration, we used the extrapolated second order BDF2 method, [9, pp. 204] or [10, pp. 197], the variable step size of which has a form of

$$\rho^m - \frac{(1+r)^2}{1+2r}\rho^{m-1} + \frac{r^2}{1+2r}\rho^{m-2} = \frac{1+r}{1+2r}\Delta\tau_m\left(2F^{m-1} - F^{m-2}\right), \quad m \geq 2, \qquad (25)$$

where superscript m denotes the time level τ_m with a step size $\Delta\tau_m = \tau_m - \tau_{m-1}$ and $r = \Delta\tau_m / \Delta\tau_{m-1}$ is the step size ratio. Here, F contains the discretized convective terms and a source term. Note, that we have dropped spatial indexes in equation (25). Since two-step method needs ρ^0 and ρ^1 as starting values, the explicit Euler method

$$\rho^m = \rho^{m-1} + \Delta t F(t_m, \rho^{m-1}) \qquad (26)$$

is used on the first step. Because of the explicit time integration, we are restricted by the standard CFL condition for stability.

The same space discretization technique (22)-(24) and time integration (25)-(26) are used also for solution to the equation for electron density (12). In this case, z-variable plays a role of 'time' in (25) and (26).

4.1.3 Poisson Equation.

To obtain a finite-difference approximation of Poisson's equations (13), (14) we use standard second order discrete scheme. To involve in calculation the jump condition (16) on the internal border, we solve Poisson equation with the source term 'zero' on semiconductor region and 'ρ' on the gas region,

$$-\frac{\varphi^m_{k,j,i-1} - 2\varphi^m_{k,j,i} + \varphi^m_{k,j,i+1}}{(\Delta x)^2} - \frac{\varphi^m_{k,j-1,i} - 2\varphi^m_{k,j,i} + \varphi^m_{k,j+1,i}}{(\Delta y)^2} - \frac{\varphi^m_{k-1,j,i} - 2\varphi^m_{k,j,i} + \varphi^m_{k+1,j,i}}{(\Delta z)^2}$$

$$= \begin{cases} 0, & \text{semiconductor layer} \\ \rho^{m-1}_{k,j,i}, & \text{gas-discharge layer} \end{cases} \qquad (27)$$

and use a discrete version of the border condition (16) at the nodes, lying on the border grid plane, instead of (27). The system of equations is solved by a symmetrical successive over-relaxation method (SSOR) (See, e.g. [10], pp.343].

4.2 Numerical Examples

Behavior, predicted by the stability analysis, can be tested on the full numerical solutions of the initial value problem: the linear stability analysis is used to determine interesting parameter regimes, and the full numerical solutions is used to explore the behavior beyond the validity of linearization.

The parameter sets at which we concentrated the analysis are dictated by the bifurcation diagram in figure 4 with the line separating regions with $\mathrm{Re}(\lambda)<0$ where the homogeneous stationary state is linearly stable from the regions with $\mathrm{Re}(\lambda)>0$ where the stationary state looses its stability [5]. We chose different positions for feeding voltage U_t at fixed resistivity R_s, from the left and right of the line, separating stable and unstable states. We give here illustrations for the two sets of parameters, distinguished by the dimensionless applied voltages U_t=23.7 and U_t=46.4 at fixed R_s=2·10^6, L=36, and L_s=54. These voltages correspond respectively to linearly stable and unstable stationary states as predicted by the bifurcation diagram in figure 4.

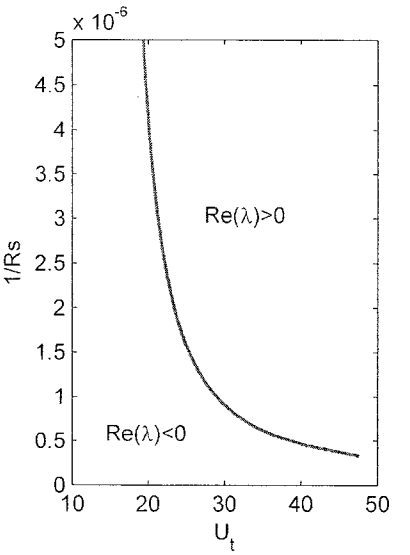

FIG. 4: Bifurcation diagram. L=36, L_s=54. [5]

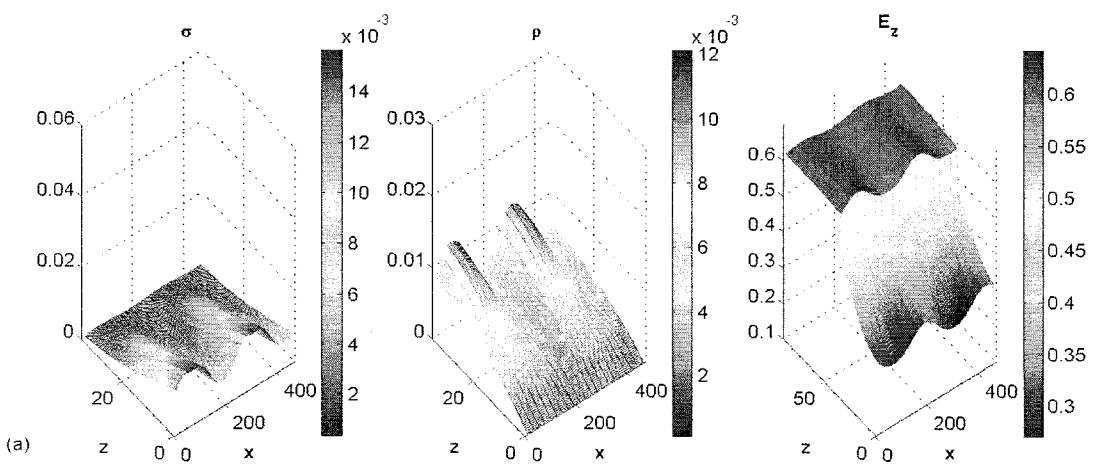

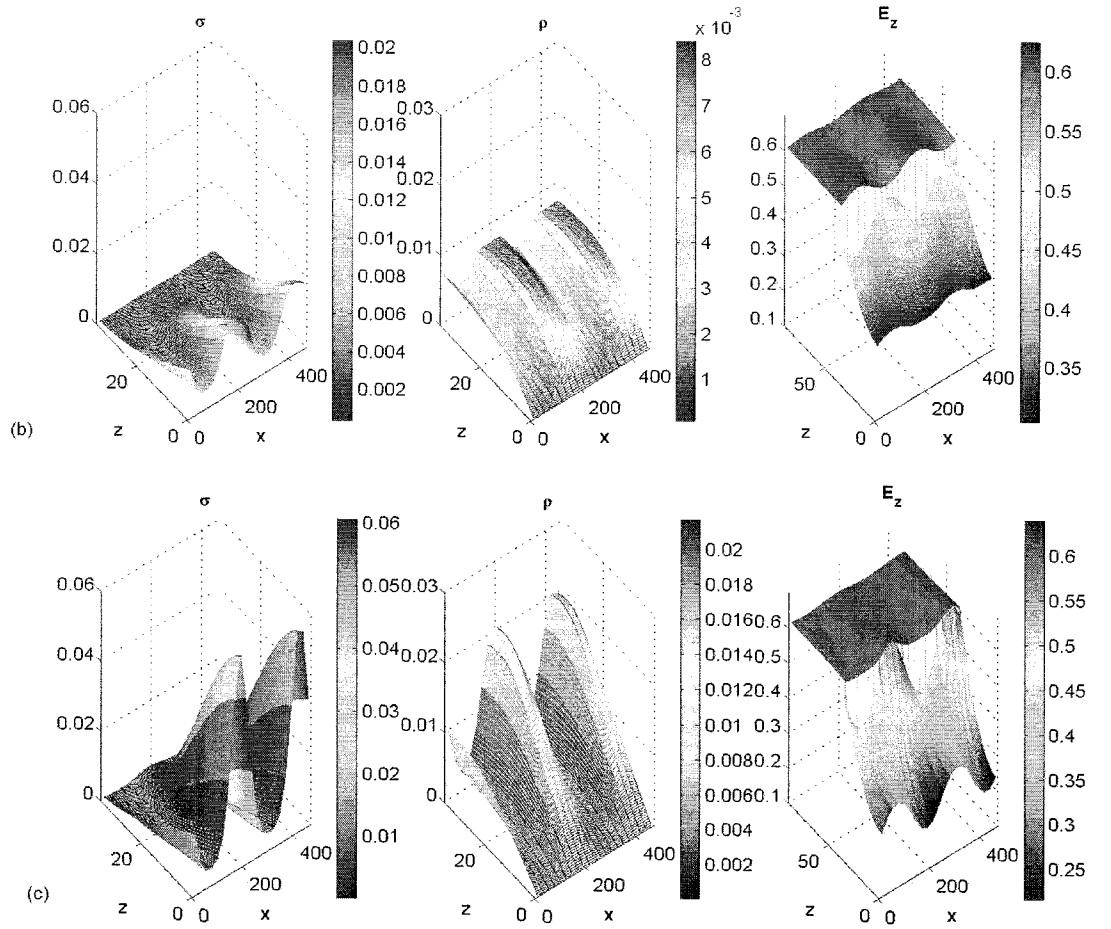

FIG. 5: Profiles and contour lines of electron and ion densities σ and ρ, and electric field component E_z. For σ and ρ, only the gas discharge part is shown, for E_z the full system. U_t=46.4, R_s=2·10^6, L=36, L_s=54. Three temporal stages of the oscillation are shown: τ=11800 (a), τ=11920 (b), and τ=12040 (c).

In figure 5, we show examples of the growing and oscillating behavior. Figure 6 presents projection of the discharge characteristics on *XY*-plane. These structures resemble the experimentally observed blinking filaments [3].

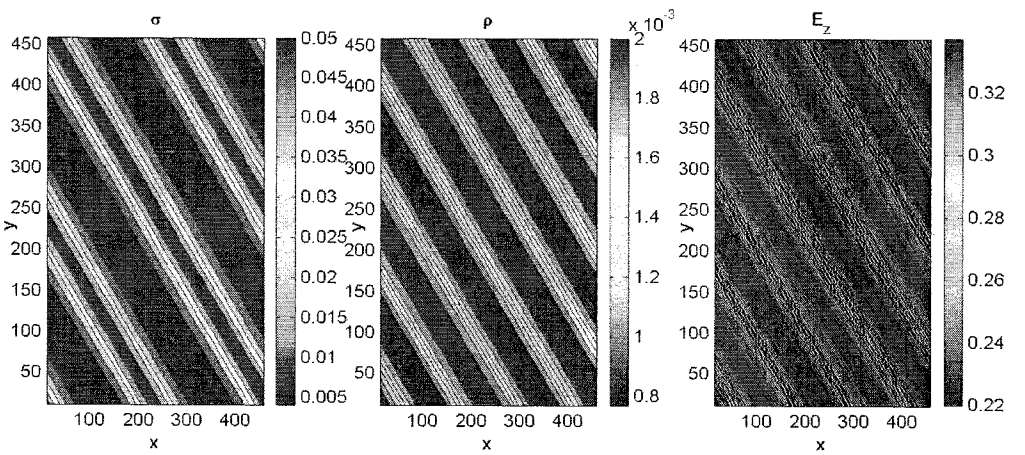

FIG. 6: Contour lines of the electron and ion densities and electric field component E_z. XY-projection. Parameters the same as in Fig. 5. Point of time τ=12040.

Figures 7 shows evolution of the ion density on the internal interface between gas and semiconductor for U_t=23.7 and U_t=46.4.

According to the stability analysis, for U_t=23.7, spatially structured oscillating mode decays: the leading mode wavenumber is k=0.050 and eigenvalue is $\lambda(k)=-0.2807\cdot10^{-3}+0.4320\cdot10^{-2}$i. Period of the temporal oscillations and characteristic wave length are predicted as $2\pi/\mathrm{Im}(\lambda)\approx454$ and $2\pi/k\approx126$. For U_t=46.4, k=0.0267 and $\lambda(k)=0.4615\cdot10^{-3}+0.1191\cdot10^{-1}$i. Since maximum of $\mathrm{Re}(\lambda(k))$ is positive now and occurred at $k\neq0$, the transversal modulation of the initial condition grows.

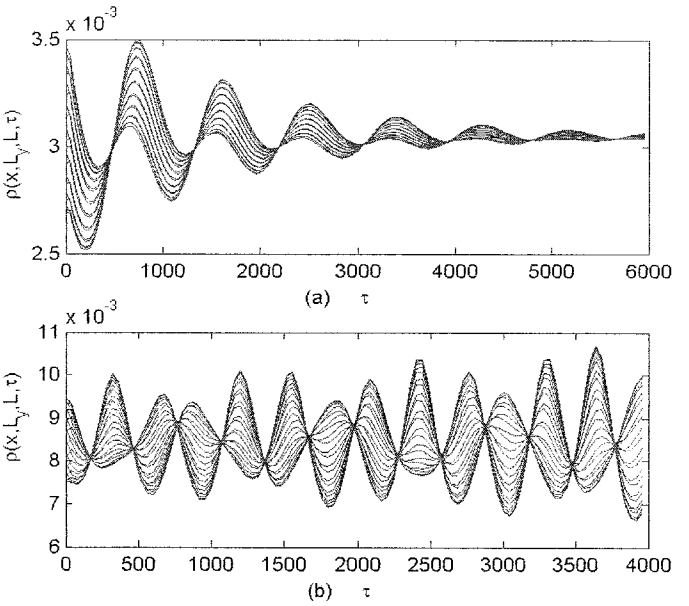

FIG. 7: Ion density ρ at the nodes of the internal border z = L as function of time. R_s=2·10^6, L=36, L_s=54, U_t=23.7 (a) and 46.4

5. Concluding Remarks

We have considered here the simplest model for the dynamical gas-discharge-semiconductor system in three spatial dimensions.

We have presented numerical solutions as well as stability analysis results of the homogenous stationary state of the system. Numerical and stability analysis results show a good agreement.

Staying within the same parameter regime as in [5], it is found that either purely Hopf bifurcation or Turing-Hopf bifurcation takes place.

References

[1] Cross, M.C. and Hohenberg, P.C. (1993) *Rev. Mod. Phys.*, 65, 851-1112.

[2] Strümpel, C., Astrov, Y.A., and Purwins, H.-G. (2000) *Phys. Rev. E*, 62, 4889-4897.

[3] Kogelschatz, U. (2003) *Plasma Chem. Plasma Process*, 23, 1.

[4] Danijela D. · Šijačić, Ute Ebert, and Ismail Rafatov (2004) *Phys. Rev. E*, 70, 056220.

[5] Danijela D. · Šijačić, Ute Ebert, and Ismail Rafatov (2005) *Phys. Rev. E*, 71, 066402.

[6] Ismail Rafatov, Danijela D. · Šijačić, and Ute Ebert, to be submitted to *Phys. Rev.* E

[7] Strümpel, C. Ph.D. thesis, Univ. Münster, Germany, 2001.

[8] Raizer, Y.P. (1997) *Gas Discharge Physics*. Berlin: Springer.

[9] Hundsdorfer, W. and Verwer, J.G. (2003) *Numerical solution of time-dependent advection-diffusion-reaction equations*, Springer Series in Comput. Math. 33. Berlin: Springer.

[10] Wesseling, P. (2001) *Principles of computational fluid dynamics*, Springer Series in Comput. Math. 29. Berlin: Springer.

[11] Thomas, J.W. (1999) *Numerical Partial Differential Equations: Conservation Laws and Elliptic Equations*, Texts in Appl. Math. 33. Berlin: Springer.